Electronic Supplementary Information (ESI)

Exciton-driven photoisomerization in photoswitch–quantum dot nanohybrids

Daniel López Díaz,[a] Gabriel Gil,[b] Stefano Corni,[c,d] and Guido Goldoni[a]

[a] *Department of Physics, Informatics and Mathematics, University of Modena and Reggio Emilia, Modena, Italy*
[b] *Department of Science and Technological Innovation, University of Eastern Piedmont, Alessandria, Italy*
[c] *Department of Chemical Sciences, University of Padova, Padova, Italy*
[d] *CNR Institute of Nanosciences, Modena, Italy*

S1. Size dependence of the QD transition electric field

In Sec. 3.2 of the main text, we noted that the matrix element $\langle \mathrm{NP}_0 | \hat{\mathbf{E}}^{\mathrm{NP}}(\mathbf{R}) | \mathrm{NP}_1^+ \rangle$ varies systematically with the quantum-dot size, providing an additional handle (beyond resonance tuning) to modulate the molecule–QD coupling in Eq. 3. Figure S1 reports the magnitude $|\mathbf{E}_{\mathrm{NP}}|$ of the $\mathrm{NP}_0 \leftrightarrow \mathrm{NP}_1^+$ spin-up transition electric-field matrix element as a function of the QD radius in the range $R_{\mathrm{QD}} = 2$–3 nm. The data are accurately described by a power-law fit, $|\mathbf{E}^{\mathrm{NP}}| = A R_{\mathrm{QD}}^{b}$, with $b \approx 2.20$ (see caption), quantifying the strong size dependence of the QD transition field in the radius window relevant for the resonance analysis of Fig. 2 of the main text.

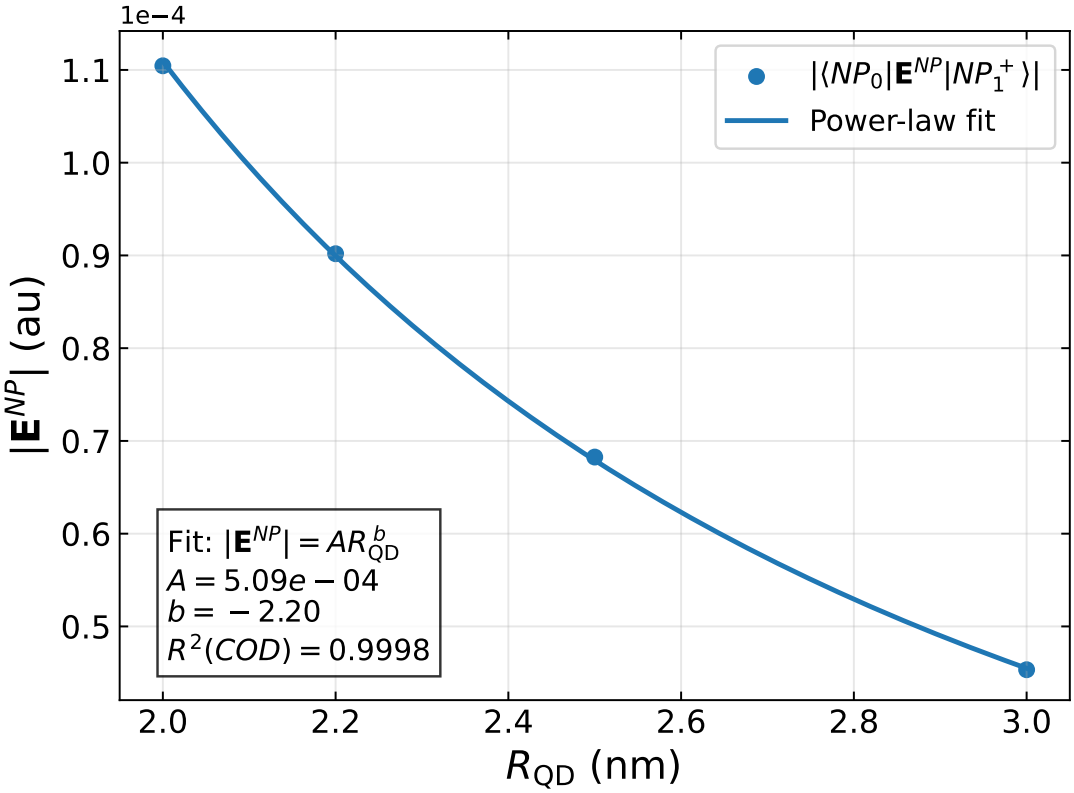

Figure S1: Electric-field magnitude $|\mathbf{E}^{\mathrm{NP}}|$ of the $\mathrm{NP}_0 \leftrightarrow \mathrm{NP}_1^+$ matrix element, as a function of the QD radius R_{QD} in the 2–3 nm range. The data follow a power-law dependence $|\mathbf{E}^{\mathrm{NP}}| = A R_{\mathrm{QD}}^{b}$ with $A = 5.09 \times 10^{-4}$, $b = 2.20$, and an excellent coefficient of determination $R^2 = 0.9998$.

S2. Orientation of molecular dipoles along the photoisomerization pathway

To substantiate the reference frame employed in the HyCI analysis, we examined the evolution of the AZB molecular dipoles along the CNNC dihedral coordinate ϕ. In the HyCI calculations, a single global rotation is defined by aligning the transition dipole $\mathbf{d}_{01}^{\mathrm{M}}$ at $\phi = 16.3^\circ$ with the laboratory z axis, and the same rotation is then applied uniformly to *all* molecular dipoles at *all* ϕ. The

analysis below provides quantitative evidence that this choice yields a consistent molecular dipole frame along the photoisomerization pathway. In particular, we verified that:

(i) the transition dipole $\mathbf{d}_{01}^{\mathrm{M}}$ maintains an approximately constant spatial direction,

(ii) the static dipoles $\mathbf{d}_{00}^{\mathrm{M}}$ and $\mathbf{d}_{11}^{\mathrm{M}}$ remain nearly orthogonal to $\mathbf{d}_{01}^{\mathrm{M}}$, and

(iii) $\mathbf{d}_{00}^{\mathrm{M}}$ and $\mathbf{d}_{11}^{\mathrm{M}}$ stay nearly parallel to each other.

Dipole magnitudes and validity of the angular analysis

The magnitudes of the three molecular dipoles $\mathbf{d}_{01}^{\mathrm{M}}$, $\mathbf{d}_{00}^{\mathrm{M}}$, and $\mathbf{d}_{11}^{\mathrm{M}}$ along the CNNC dihedral angle ϕ are shown in Fig. S2. Near the *trans* ($\phi = 180^\circ$) configuration, $|\mathbf{d}_{ij}^{\mathrm{M}}|$ approaches zero, which would render angular quantities ill-defined. To avoid numerical noise arising from these regions, all angular quantities discussed below were evaluated only when the corresponding dipole modulus satisfied

$$|\mathbf{d}_{ij}^{\mathrm{M}}(\phi)| \geq 0.1\,|\mathbf{d}_{01}^{\mathrm{M}}(16.3^\circ)|.$$

The dashed line in Fig. S2 indicates this global threshold, which removes only geometries where the dipole orientation loses physical meaning while preserving the entire dynamical region relevant for photoisomerization.

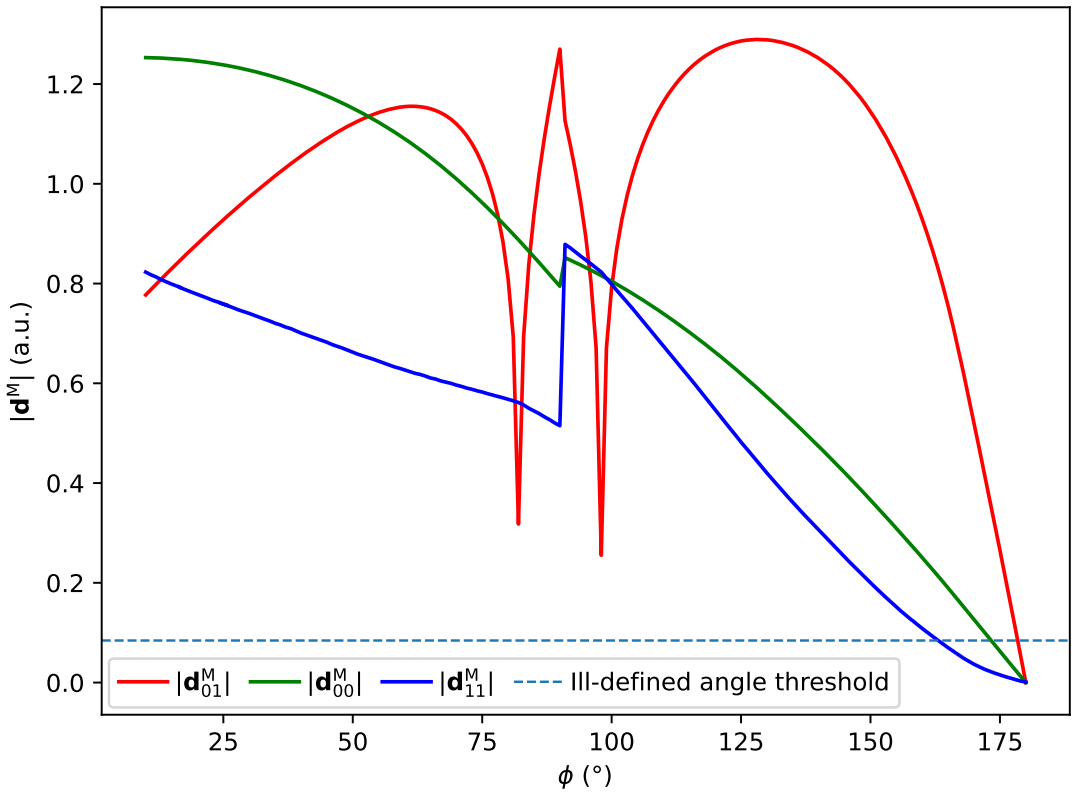

Figure S2: Magnitudes of $\mathbf{d}_{01}^{\mathrm{M}}$, $\mathbf{d}_{00}^{\mathrm{M}}$, and $\mathbf{d}_{11}^{\mathrm{M}}$ along the CNNC dihedral angle ϕ. The dashed line denotes the global threshold used to exclude geometries with ill-defined dipole orientations.

Stability of the transition dipole direction

Figure S3 shows the sign-invariant angle between $\mathbf{d}_{01}^{\mathrm{M}}(\phi)$ and the reference vector $\mathbf{d}_{01}^{\mathrm{M}}(16.3^\circ)$, evaluated only within the valid magnitude region defined above. The angular deviation remains below $\sim 8^\circ$ across the entire accessible interval, demonstrating that the transition dipole direction is essentially rigid along the photoisomerization pathway.

Orthogonality of static dipoles to the transition dipole

The deviations from perfect orthogonality between $\mathbf{d}_{00}^{\mathrm{M}}$ or $\mathbf{d}_{11}^{\mathrm{M}}$ and $\mathbf{d}_{01}^{\mathrm{M}}$ are displayed in Fig. S4. Both remain below $\sim 0.6^\circ$, indicating an essentially perpendicular arrangement throughout the photoisomerization coordinate.

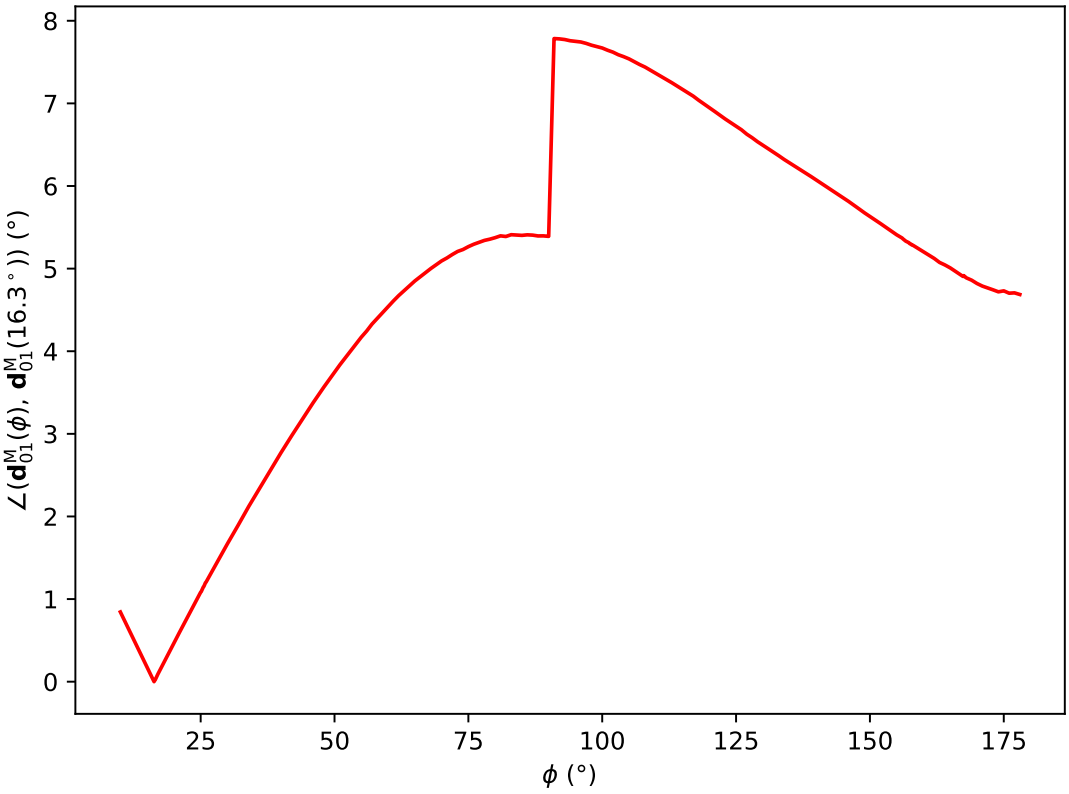

Figure S3: Sign-invariant angular deviation between $\mathbf{d}_{01}^{\mathrm{M}}(\phi)$ and $\mathbf{d}_{01}^{\mathrm{M}}(16.3^\circ)$ along the CNNC coordinate ϕ, evaluated above the global magnitude threshold. The small angular spread confirms the near-constancy of the transition dipole direction.

Parallelism of the static dipoles

Figure S5 reports the direct angle between $\mathbf{d}_{00}^{\mathrm{M}}$ and $\mathbf{d}_{11}^{\mathrm{M}}$. The angle stays below $\sim 1^\circ$ across the valid region, demonstrating that the two static dipoles remain essentially parallel along the entire pathway.

Overall, these results demonstrate that the AZB molecular dipole frame behaves as a nearly rigid orthogonal triad along the photoisomerization coordinate. This geometric robustness underpins the validity of the dipole-based alignment procedure used in the HyCI description of the PhS–QD nanohybrid.

S3. Convergence of the excitonic splitting with respect to the HyCI basis cutoff

To assess the numerical sensitivity of the excitonic splitting, we monitored the energy difference between the two adiabatic states of interest, Ψ_1 and Ψ_2, at the avoided crossing near $\phi = 16.3^\circ$ for different sizes of the hybrid basis set.

The size of the hybrid basis set is controlled via an energy cutoff parameter, such that molecule-NP couplings are retained only if the involved fragment states have independent energies below the cutoff. We scanned the cutoff between 3.2 and 6.4 eV in increments of 0.1 eV. The largest basis set explored, corresponding to $E_{\mathrm{cut}} = 6.4$ eV, contains 58 435 states. For each basis set, we performed a HyCI calculation and evaluated the excitonic splitting $\Delta E_{\mathrm{split}}(E_{\mathrm{cut}}) = \left| E_{\Psi_2}(E_{\mathrm{cut}}) - E_{\Psi_1}(E_{\mathrm{cut}}) \right|$.

The resulting curve (see Fig. S6) shows that the splitting is essentially stable over the scanned range, varying only between ~ 4.274–4.281 meV. A sigmoid fit is included solely as a visual guide to emphasize the convergence trend with increasing E_{cut}. As a conservative estimate of the intrinsic truncation error, we take the difference between the last and first sampled values, $\Delta E_{\mathrm{split}}(E_{\mathrm{cut}}^{\mathrm{max}}) - \Delta E_{\mathrm{split}}(E_{\mathrm{cut}}^{\mathrm{min}}) \approx 5 \times 10^{-3}$ meV, which is more than two orders of magnitude smaller than the excitonic splitting reported in the main text.

Since increasing the cutoff can only introduce additional HyCI configurations and coupling pathways, the observed increase of the splitting at larger values of E_{cut} implies that the reported results, obtained for a lower cutoff of $E_{\mathrm{cut}} = 3.2\ eV$, should be regarded as a conservative lower bound for the exact excitonic splitting.

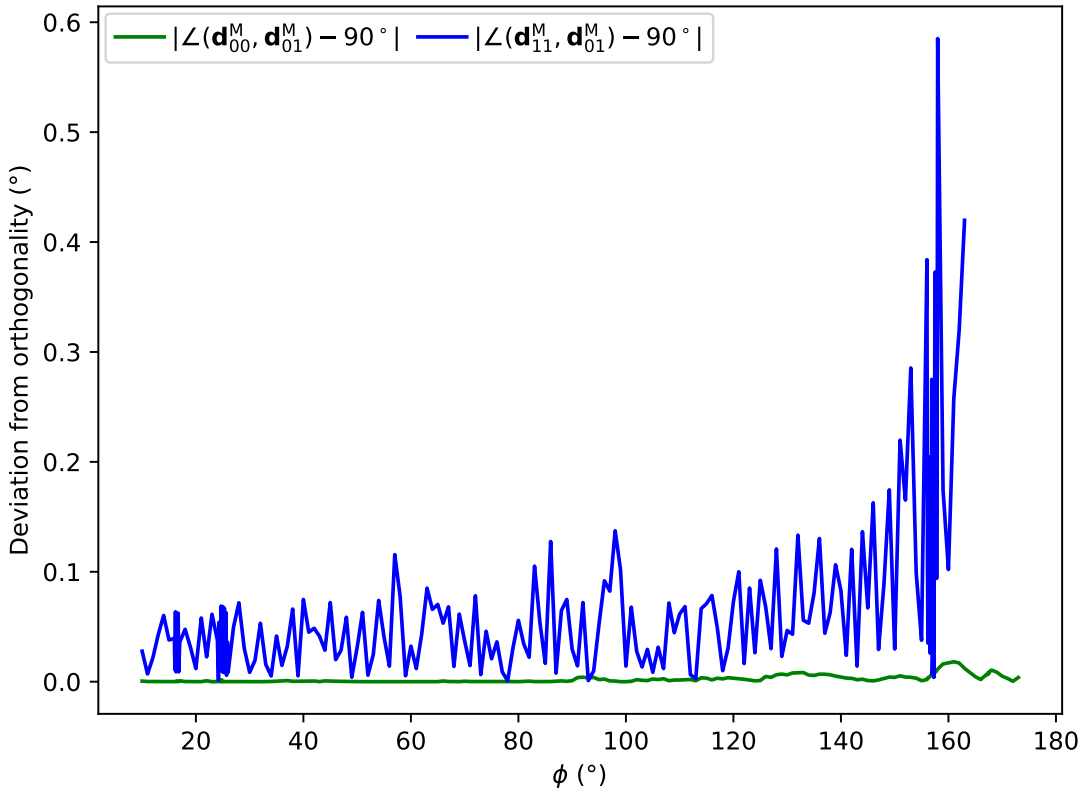

Figure S4: Deviation from orthogonality between the static dipoles $\mathbf{d}^{\mathrm{M}}_{00}$, $\mathbf{d}^{\mathrm{M}}_{11}$ and the transition dipole $\mathbf{d}^{\mathrm{M}}_{01}$ along ϕ, evaluated above the global magnitude threshold. The deviations remain below $\sim$0.6°, confirming persistent perpendicularity.

S4. Zoom of the avoided crossing near $\phi \approx 167.7^\circ$

In Sec. 3.3, the hybrid PESs of Fig. 5 show two avoided crossings, located near $\phi \approx 16.3^\circ$ and $\phi \approx 167.7^\circ$, where the AZB $M_0 \rightarrow M_1$ excitation becomes nearly resonant with the lowest bright QD exciton (NP_1). While the first avoided crossing is analyzed in detail in Fig. 6, Figure S7 provides the corresponding zoom around $\phi \approx 167.7^\circ$. As in Fig. 6, the coupled ($V^{\mathrm{M-NP}} \neq 0$) and uncoupled ($V^{\mathrm{M-NP}} = 0$) cases are shown together to make the level repulsion apparent and to confirm that the gap arises from genuine hybridization between the $|M_1, \mathrm{NP}_0\rangle$ and $|M_0, \mathrm{NP}_1\rangle$ diabatic states. Notably, the magnitude of the splitting at this second avoided crossing is comparable to that observed near $\phi \approx 16.3^\circ$, amounting to approximately $\sim$3.5 meV versus $\sim$4 meV, respectively.

S5. Additional discussions in the nanohybrid model

Effect of multiple resonant QD excitonic states

In the resonance regime discussed in the main text, we focused on the minimal case in which a single bright QD exciton falls within the energy window defined by the AZB $M_0 \rightarrow M_1$ transition. Here we briefly discuss the more general situation in which multiple QD excitonic states lie within the same resonance window.

When several QD excitons become energetically resonant with the molecular excitation, the hybridization scenario becomes correspondingly richer. Multiple QD excitations can simultaneously couple to the molecular transition, leading to a manifold of interacting hybrid states. Along the photoisomerization pathway, this results in multiple avoided crossings rather than a single well-isolated one.

In such a regime, the redistribution of oscillator strength and dipole character occurs over several hybrid states, potentially producing a more intricate pattern of exciton–molecule mixing. These multi-state resonance effects are naturally accounted for within the HyCI framework, which treats all resonant fragment excitations on equal footing.

The present work deliberately concentrates on the minimal single-resonance case in order to isolate and clearly interpret the fundamental mechanisms underlying exciton-driven photoisomerization.

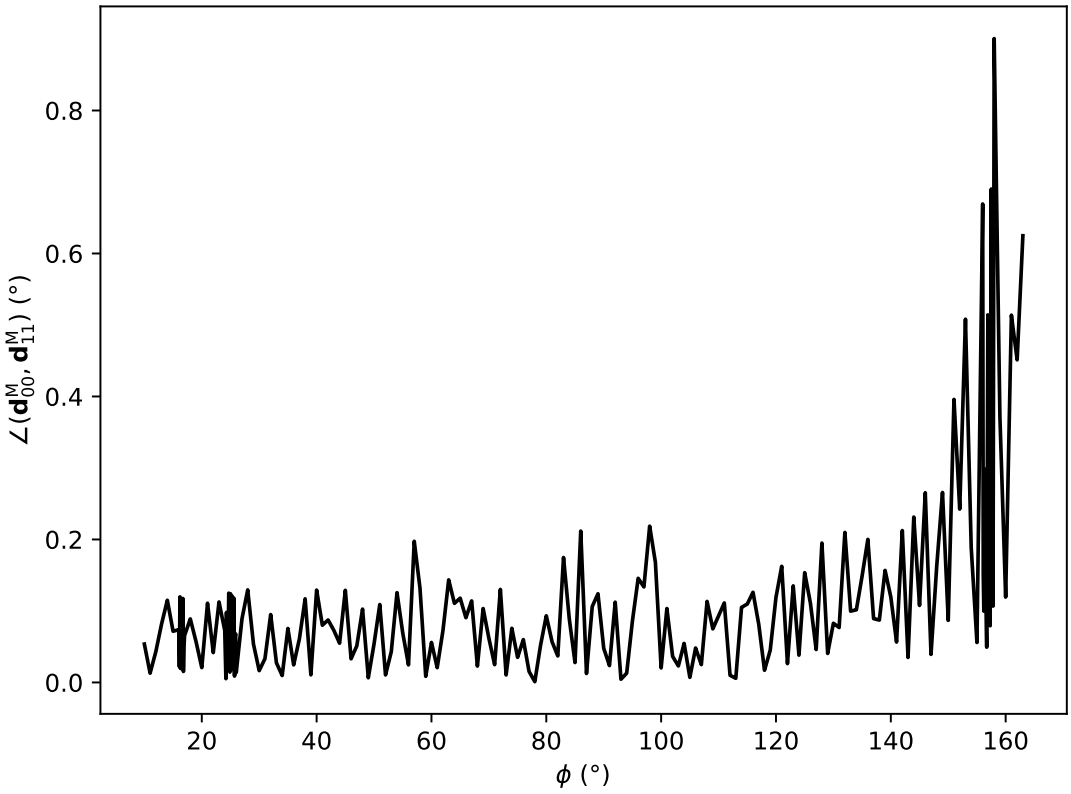

Figure S5: Angle between $\mathbf{d}_{00}^{\mathrm{M}}$ and $\mathbf{d}_{11}^{\mathrm{M}}$ along the CNNC coordinate, evaluated above the global magnitude threshold. The near-zero angle indicates persistent parallel alignment of the static dipoles.

Expected behavior for multiple azobenzene molecules

In the single-molecule nanohybrid considered in this work, the magnitude of the excitonic splitting is primarily governed by the quantum dot, which provides the dominant excitonic degree of freedom interacting with the molecular excitation.

If the number of azobenzene molecules coupled to the same QD were increased, the system would in general become more complex due to the presence of multiple molecular excitations and possible collective effects. A quantitative description of such a scenario would require additional modeling assumptions and explicit calculations, and is therefore beyond the scope of the present study.

Our work deliberately focuses on experimentally accessible nanohybrids consisting of a single quantum dot coupled to a single molecule. Within this well-defined and practically realizable regime, the avoided-crossing mechanism, the role of resonance, and the tunability via QD properties remain valid, and the overall conclusions of this work are not expected to change.

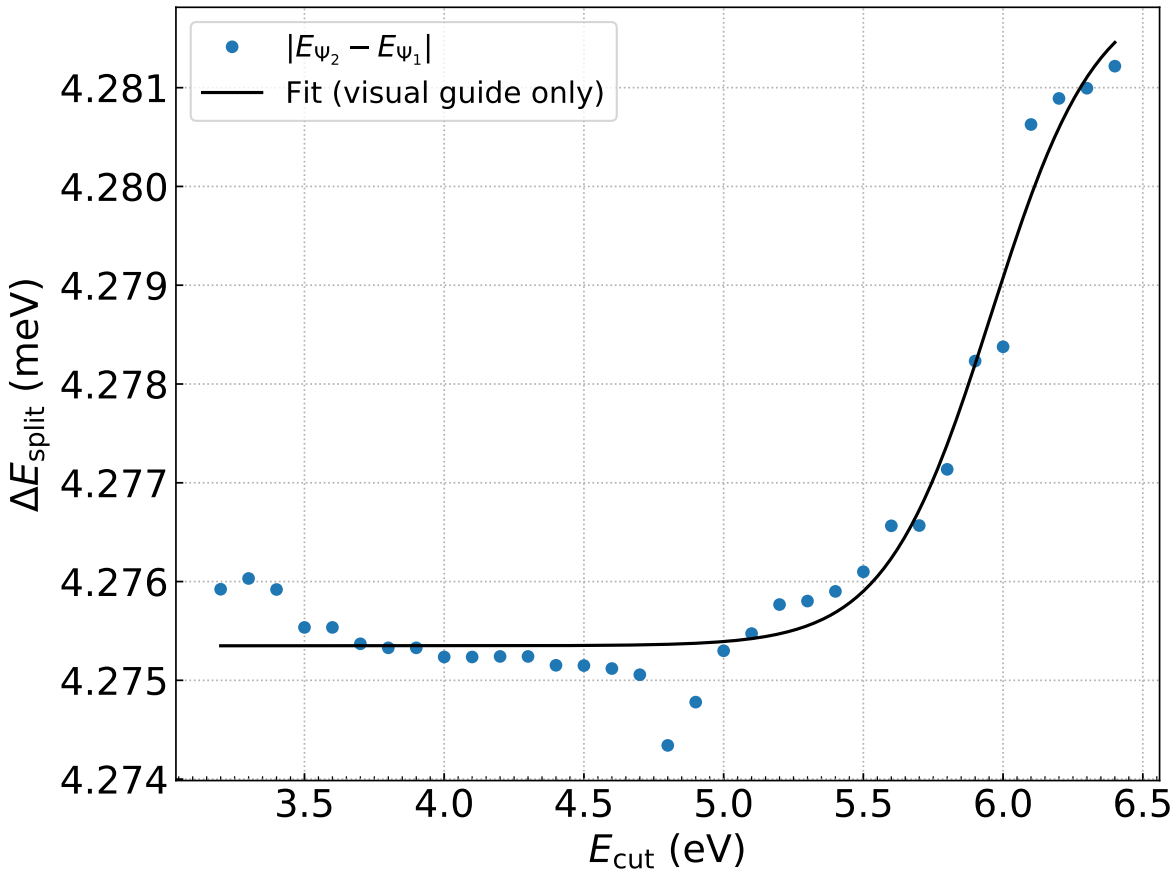

Figure S6: Dependence of the excitonic splitting $\Delta E_{\mathrm{split}} = \left|E_{\Psi_2} - E_{\Psi_1}\right|$ at the avoided crossing near $\phi = 16.3^\circ$ for the AZB–CdSeQD nanohybrid considered in the main article, as a function of the energy cutoff parameter E_{cut}. A sigmoid fit is shown only as a visual guide to highlight the convergence trend. The splitting remains stable over the scanned range, varying between ~ 4.275 and ~ 4.281 meV.

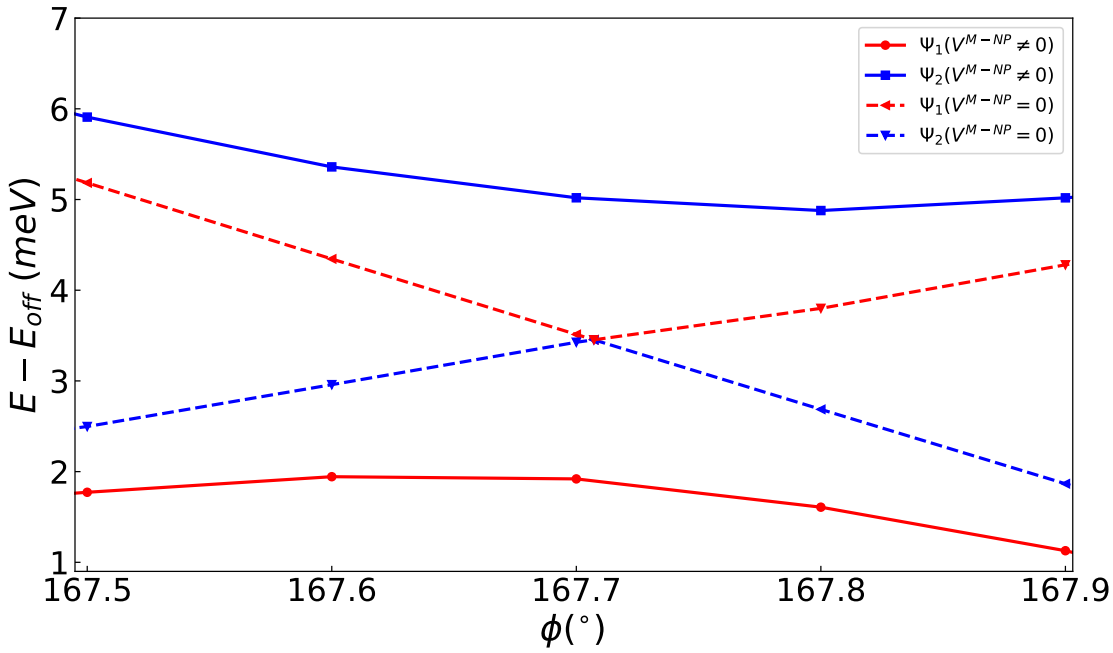

Figure S7: Zoomed view of the hybrid PESs around the avoided crossing near $\phi \approx 167.7^\circ$ for the AZB–CdSeQD system with $R_{\mathrm{QD}} = 2.2$ nm and $\mathbf{R} = (0, 0, 2.931)$ nm. Solid and dashed curves correspond to the coupled and uncoupled cases, respectively, highlighting the level repulsion induced by the excitonic coupling. The plot is reported on a relative (meV) scale using the same zooming strategy adopted in Fig. 6 of the main text.